SERBIAN JOURNAL OF ELECTRICAL ENGINEERING
Vol. 21, No. 2, June 2024, 251-273
UDC: 621.391.826:[612.23:621.3.013.1 **DOI: https://doi.org/10.2298/SJEE2402251R**

Wavelet Transform Generated Inherent Noise Reference for Adaptive Filtering to De-noise Pulse Oximeter Signals

Bondala Venumaheswar Rao [1], Ette Hari Krishna[2], Komalla Ashoka Reddy[3]

Abstract: As exemplified during the COVID-19 pandemic and in post-operative intensive care units, monitoring blood oxygen saturation (SpO_2) levels is crucial in terms of assessing a patient's health condition. Due to random movements of the subject, a pulse-oximeter-driven photoplethysmographic (PPG) signal becomes noisy while recording, with motion artefacts (MAs), which will disturb the morphological features, leading to incorrect SpO_2 levels. The MA noise may contain either low- or high-frequency components, resulting in a scenario with in-band and out-of-band noise. The reduction of in-band noise with an adaptive filter requires a reference signal, and an additional sensor such as an accelerometer is normally used in addition to the PPG sensor to capture the MAs. The present work focuses on the generation of a reference for inherent noise using a wavelet transform (WT), thereby eliminating the need for an external sensor. The computed values of the correlation coefficient and magnitude squared coherence are used to establish the validity of the generated inherent noise reference. Our WT-driven adaptive filtering method reduces MAs, simplifies the correct approximation of the SpO_2 and heart rate, and also restores the respiratory components. The de-noised PPG signals presented here and a corresponding numerical study prove the usefulness of the proposed method, which has a worst-case accuracy of 0.5% in regard to SpO_2 estimations.

Keywords: Wavelet transform, Pulse oximeter, PPG signal, Motion artifact, blood oxygen saturation (SpO_2), In-band noise, Out-of-band noise, Inherent noise reference, LMS adaptive filter.

1 Introduction

Pulse-oximeter-driven photoplethysmographic (PPG) signals are used [1– 4] to monitor important physical parameters such as blood oxygen saturation (SpO_2), respiratory information, and heart rate. A PPG sensor acquires red (R)

[1]Assistant Professor of E&I Engineering, KITS, Warangal, Telangana, India; E-mail: bvm.eie@kitsw.ac.in
[2]Assistant Professor of ECE, UCE, KU, Kothagudem, Telangana, India; E-mail: hari_etta@kakatiya.ac.in
[3]Professor of ECE, KITS, Warangal, Telangana, India; E-mail: kareddy.iitm@gmail.com

and infra-red (IR) PPG signals. Accurate and reliable estimations of SpO_2 levels play an important role in monitoring health conditions, as especially apparent during the COVID-19 pandemic and in post-operative intensive care units. The accurate estimation of these important parameters depends on the quality of pulse-oximeter-driven PPG signals. In general, a PPG signal can become corrupted with motion artefacts (MAs), resulting in an erroneous estimation of SpO_2. The spectrum of PPG signals consists of frequencies of 0 to 4 Hz, including the ECG synchronised pulse signal (0.8 Hz to 2 Hz), and respiratory information (0.2 Hz to 0.33 Hz). MA noise may include an in-band or out-of-band frequency component.

In the literature, many methods have been proposed to reduce MAs in PPG signals. One method [5] combined multi-resolution analysis based on a wavelet transform (WT) with the Mallat algorithm, and was found to determine the pulse amplitude accurately and to detect MAs in the pulse wave. An adaptive comb filtering method with an adaptive lattice IIR notch filter technique [6] was also proposed to reduce MAs in PPG signals. To improve the performance of PPG sensors, a technique based on an LMS adaptive noise canceller [7] was put forward to assess the fundamental frequency and generate a synthetic noise signal for reference.

To eliminate the MA noise from PPG signals, a new method based on a combination of a constrained independent component analysis algorithm and an adaptive filter was used in [8]. Another method [9] that involved cycle-by-cycle Fourier series analysis was used for the compression and de-noising of PPG signals. A data-driven Hilbert transform based on empirical mode decomposition (EMD) was applied to reduce the MAs in PPG signals, with its basic decomposing feature as intrinsic mode functions (IMFs) [10]. In addition to this method, multi-scale empirical mode decomposition (MS-EMD) can be used with wavelet processing and empirical mode decomposition concepts to reduce the MAs in PPG signals [11].

A method based on a periodic moving average filter [12] was developed in which the quasi-periodicity of the PPG signals was exploited to remove MAs. The moving average method was not found to remove MAs with large amplitudes. An algorithm based on a dual-tree complex WT and morphological filtering was also presented for de-noising the PPG signal, and was shown to effectively remove high-frequency noise [13]. A comb filter was designed based on the estimated period of the PPG signal [14], and was used to filter out MAs from band-pass filtered PPG signals. A novel technique [15] was proposed for accurately reconstructing motion-corrupted heart rate signals using a PPG sensor based on spectral filter algorithm for MA and heart rate reconstruction. An approach was presented for determining the heart rate by reducing the MA from the PPG signal using singular value decomposition and filtered X-LMS [16]. A

new concept was developed in which an artificial neural network (ANN) was used to restore the morphology of the PPG signal while reducing the MAs [17]. An LMS-Newton adaptive filter method based on the estimation of the fundamental frequency was also put forward to diminish the effect of MAs on pulse oximeter data [18]. Three algorithms, called the ICA-adaptive filter algorithm, Butterworth ICA-adaptive filter algorithm, and Butterworth-wavelet transform algorithm, were developed to eliminate the effect of MAs [19]. A multi-channel spectral matrix decomposition model was proposed to predict heart rate in the presence of vigorous physical activity. The elimination of MAs was first modelled as a spectral matrix decomposition optimisation issue, and a new spectral peak detection approach was then applied to calculate the heart rate when motion disturbances had been minimised [21]. A new signal processing framework was described in [22] that employed a two-channel PPG signals to estimate heart rate in two steps: the first step used an absolute criterion condition based on ensemble EMD to eliminate the potential run-away errors, while the second step strengthened the algorithm's robustness against off-track errors. A generic algorithm [23] was proposed for a beat-to-beat analysis for artefact-reduced PPG signals after the removal of periodic motion artifacts. The suggested approach was useful for monitoring the activities of daily living, cardio-pulmonary exercise testing, and cardiopulmonary resuscitation.

A variational mode decomposition and Hilbert transform approach have also been presented [24] to estimate the pulse rate from an MA-corrupted PPG signal, and the acquired IMFs were used to construct the associated marginal spectrum. A method based on the time-frequency components of the PPG signal [25] was proposed to compute the arterial oxygen saturation; in this approach, a 22-minute dataset was acquired from 10 participants during voluntarily induced hypoxia, with and without subject-induced MAs. An envelope filtering and time-delay neural network have also been applied to a single-noise interaction model for MA removal under conditions of rigorous physical exercise [26]. A fusion-based technique was proposed in [27] to eliminate MAs from the PPG signal. This technique required the use of a PPG sensor and accelerometer data at the same time. Signal-quality assessment-guided compression of the PPG signal using an improved gain shaped vector quantisation technique [28] was explored in regard to monitoring the health conditions of patients. In this method, kurtosis and autocorrelation parameters were computed to identify good-quality pulse signals, and a deep auto encoder was used to minimise the percentage root-mean-squared difference error. A new approach was also developed to reduce the MAs in a PPG signal using the ambient light contribution as a reference [29].

In this paper, we propose an effective adaptive technique for de-noising a PPG signal. In general, an adaptive filter requires a reference signal for its operation, and the majority of adaptive-filter-based MA reduction signal processing methods have employed an additional sensor [31–33], typically an

accelerometer sensor, to capture the MAs, and have used this as reference signal. This approach leads to high power consumption and problems associated with the integration of accelerometer and PPG sensor [34]. In contrast, we propose a method that inherently generates the noise reference from the corrupted PPG signal, thereby dispensing with the need for an additional sensor. WT processing of the noisy PPG signal provides a way to obtain a secondary noise reference signal for adaptive filtering. The proposed technique de-noises the PPG signal while restoring essential physiological parameters such as the heart rate and respiratory rate, in addition to enabling a reliable estimation of SpO_2. This work represents an extension to a previous paper presented at a conference [30].

2 Method

Adaptive filtering will be always the best approach in circumstances where desired and undesired signals are in the same frequency band. The presence of MAs in a PPG signal is an example of such a scenario, and adaptive filtering therefore offers the best solution. Our objective is to develop a method to eliminate the noise from PPG signals using adaptive filtering, where the secondary noise is inherently generated from the corrupted signal using a WT method, as shown in Fig. 1.

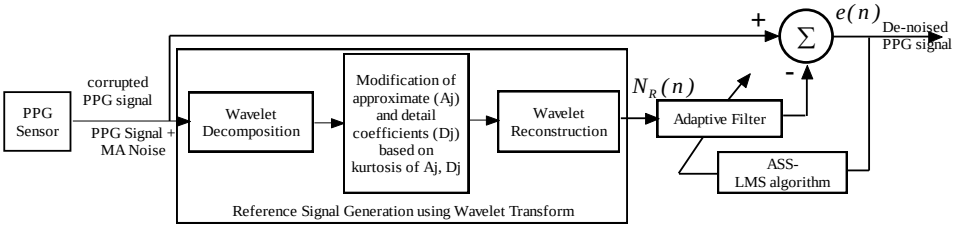

Fig. 1 – *Block diagram showing the generation of an inherent noise reference signal using a wavelet transform for adaptive filtering, to eliminate the noise from PPG data.*

2.1 Adaptive filtering

In general, adaptive filtering methods alter the filtering coefficients based on different self-adjusting algorithms in order to eliminate undesired signals that are in the same frequency band as the desired signal. With the aim of reducing the minimum mean square error, different variants of LMS algorithms have been developed to converge in fewer iterations. The conventional LMS algorithm equations are given below.

The output of a LMS adaptive filter, as given in [20], is

$$y[n] = w^{\mathrm{T}}[n]x[n], \tag{1}$$

where $x[n]$ is the input, $y[n]$ is the output, $d[n]$ is the desired output, $w[n]$ is the filter weight vector, $e[n]$ is the error, and μ is the step size.

The error is given by

$$e[n] = d[n] - y[n]. \tag{2}$$

Based on this error term, the weight vector update equation is

$$w[n+1] = w[n] + \mu e[n]x[n]. \tag{3}$$

The adaptive step size LMS (AS-LMS) algorithm [20] has been proven to be an effective LMS algorithm, as it requires fewer iterations to converge compared with other variants. The convergence parameter is adaptively modified by the introduction of a gradient vector, as follows:

$$\mu[n+1] = \mu[n] + \rho e[n]\xi^H[n]u[n], \tag{4}$$

where ρ is a positive constant used to control updating of the step size, and

$$\xi^H = \text{gradient vector} = \frac{\partial w(n)}{\partial \mu(n)}. \tag{5}$$

The reference signal is an essential aspect of an LMS algorithm for an adaptive filter. In the following section, we explain how the reference signal is inherently generated from the noisy PPG signal, thus avoiding the need for an additional sensor.

2.2 Wavelet transform

Pulse oximeter PPG signals are periodic, with a time-varying period. A WT gives both time and frequency information on the signal at the same time, and is used to analyse non-stationary signals. Equation (6) shows the WT of a given signal $f(t)$ with a suitable mother wavelet window $\psi(t)$ [5],

$$F(s,d) = \frac{1}{\sqrt{s}} \int_{-\infty}^{\infty} \psi\left(\frac{t-s}{d}\right) f(t)\,\mathrm{d}t, \tag{6}$$

where s is the time-shifting parameter, and d is the time-scaling parameter.

With considering appropriate filters, a discrete wavelet transform (DWT) decomposes the PPG signal into the corresponding approximate (A_j) and detail coefficients (D_j). The noise reference signal can be generated by suitably modifying the values of A_j and D_j, as described below.

2.2 Generation of the Inherent Noise Reference Signal

The process used to generate a wavelet-transform-driven inherent noise reference (INR) from a noisy PPG signal is summarised below.

i. By applying wavelet decomposition, the recorded noisy PPG data are decomposed into equivalent approximate (A_j) and detail coefficients (D_j).

ii. The signal randomness is taken as the measure for identifying the MAs. The kurtosis (*ku*), which is used here as a measure of the randomness of a signal $x(t)$, is given by:

$$ku = \frac{E\left(x-\mu\right)^4}{\sigma^4}, \tag{7}$$

where μ and σ are the mean and standard deviation of $x(t)$, respectively. Based on the computed kurtosis values, the signal, noise and a combination of signal and noise can be identified.

iii. To generate an INR, the approximate and detail coefficients of the PPG signal are altered using the following methodology.

Based on the kurtosis values of coefficients A_j and D_j values, the following can be inferred:

a. A very high kurtosis indicates that the random constituents represent out-of-band MA noise, and we therefore keep the corresponding coefficients A_j and D_j unmodified.

b. Moderate kurtosis values for the decomposed A_j and D_j indicates that these correspond to a blend of the desired PPG data with undesired in-band noise. Thresholding is therefore applied to the A_j and D_j coefficients to obtain the INR signal.

c. Low kurtosis values indicate that the constituents correspond to periodic pulsatile constituents. In this case, A_j and D_j are set to zero.

iv. These steps enable clear identification of the in-band and out-of-band MA noise. Finally, the INR signal is generated using the A_j and D_j constituents that have been altered as described above.

An implementation of these steps, which were to generate the INR signal component, is presented in the following sections.

3 Results

The pulse oximeter data used for our experiments were acquired from various volunteers in our research laboratory using a BIOPAC system, as illustrated in Fig. 2. Following a pre-defined protocol, PPG signals were acquired and MAs were intentionally added.

Signals were recorded in a fashion that acquired signal should consist of noise frequency as in-band and out-of-band of interest. Volunteers first gave their signed, written consent to this process.

(a)

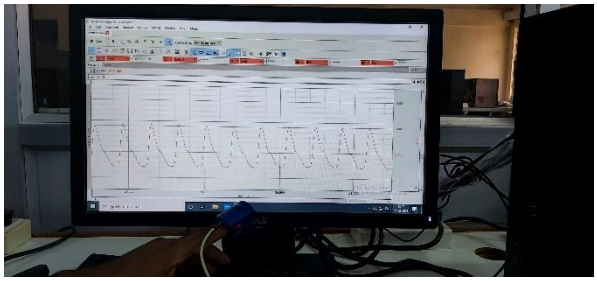

(b)

Fig. 2 – (*a*) *Setup used for BIOPAC PPG experiments;*
(*b*) *A record of pulse oximeter data.*

3.1 PPG normalisation

In order to obtain a reference signal, the PPGs were first normalised for the purpose of investigation. To achieve this, 10 cycles of PPG data were considered, and the corresponding values of the mean and variance were calculated.

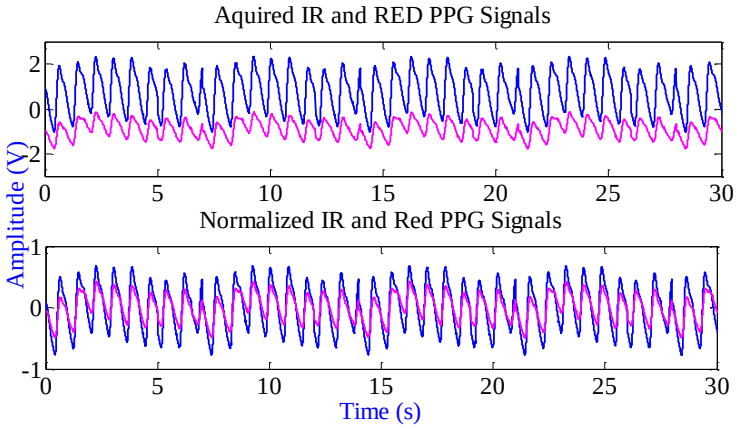

Fig. 3 – *Recorded and corresponding normalised PPG data.*

Finally, to obtain the reference signal, the mean was subtracted and the variance was divided over the 10 cycles of PPG data. The recorded and normalised PPG data are shown in Fig. 3.

3.2 Generation of the Inherent Noise Reference Signal

After wavelet decomposition of the normalised PPG signal, the kurtosis of the approximate and detail coefficients was exploited as a measure of the randomness. We can consider three cases:

Case 1: If the data are either periodic or quasi-periodic in nature, the kurtosis value will be close to three. In this case, the A_j and D_j coefficients are set to zero.

Case 2: If the data represent a combination of either periodic or quasi-periodic components with random noise, the kurtosis values will be greater than three and less than or equal to 10. In this case, thresholding is applied to the A_j and D_j coefficients to obtain the INR.

Case 3: If the data contain purely random components, the kurtosis value will be above 10. In this case, the coefficients A_j and D_j are unaltered.

Fig. 4 displays pseudocode for the INR signal generation algorithm based on a wavelet transform.

i. If only out-of-band noise is present in the signal $x_1(n)$

The kurtosis values for the approximate (A_j) and detail (D_j) coefficients for an eight-level decomposed vector $x_1(n)$ are presented in **Table 1**. Here, the kurtosis of the detail coefficient D_4 is close to three, this representing a periodic component. In this case, the component is the PPG pulsatile component.

Table 1
Kurtosis values for the approximate and detail coefficients, for out-of-band noise only.

Coefficient	Kurtosis
D_1	29.46
D_2	26.73
D_3	19.29
D_4	**2.89**
D_5	2.21
D_6	2.33
D_7	2.47
D_8	2.11
A_8	2.68

The kurtosis values for the detail coefficients D_1, D_2 and D_3 are very high, indicating that these are out-of-band noise coefficients. The remaining kurtosis values are lower than three, representing other important signal components with some periodic nature.

Pseudocode: Inherent noise reference signal generation algorithm
Input: *PPG signal from sensor*
Output: *Inherent noise reference signal*

Preprocessing: PPG signal normalisation
//N- level Wavelet decomposition on normalised PPG signal //
N=8;
[Aj, Dj]= wavelet decom (normalised PPG signal, N levels)
// Kurtosis computation for Aj, Dj //
Compute the kurtosis of coefficients Dj
for j=1:N
    Compute the kurtosis of coefficients D_j
end
Compute the kurtosis of coefficients A_N
// Modify Aj , Dj for three cases//
for k=1:N
    if kurtosis(D_k)>10 & kurtosis(D_k)<100
        Reset the values of D_k
        else if kurtosis(D_k)>3 & kurtosis(D_k)<10
            Apply thresholding to D_k
            else if kurtosis(D_k) ≤ 3
                Set D_j to all zeros
            End
End
for m=N;
if kurtosis(A_m)>10 & kurtosis(A_m)<100
    Reset the values of A_m
    else if kurtosis(A_m)>3 & kurtosis(A_m)<10
        Apply thresholding to A_m
        else if kurtosis(A_m) ≤ 3
            Set A_m to all zeros
        End
End
// N- level wavelet reconstruction on modified A_N and D_1 to D_N //
Noise reference=WaveRecon(modified Aj, Dj)

Fig. 4 – *Pseudocode for the inherent noise reference signal generation algorithm.*

The detail coefficients D_1, D_2, D_3 therefore represent the noise present in the signal $x_1(n)$. So, to extract, noise reference, except D_1, D_2, D_3 (representing out-of-band noise), the values of all the other coefficients will be forced to zero.

Wavelet reconstruction is then applied to the modified coefficients to obtain a noise reference signal for the adaptive filtering process.

The AS-LMS algorithm is employed to de-noise the PPG signal using this inherently generated noise reference signal. The results discussed above are shown in Fig. 5. The PPG signal corrupted with out-of-band noise is presented Fig. 5a, while the WT-generated inherent out-of-band noise is shown in Fig. 5b and the corresponding PPG signal after de-noising using the proposed adaptive filter is shown in Fig. 5c.

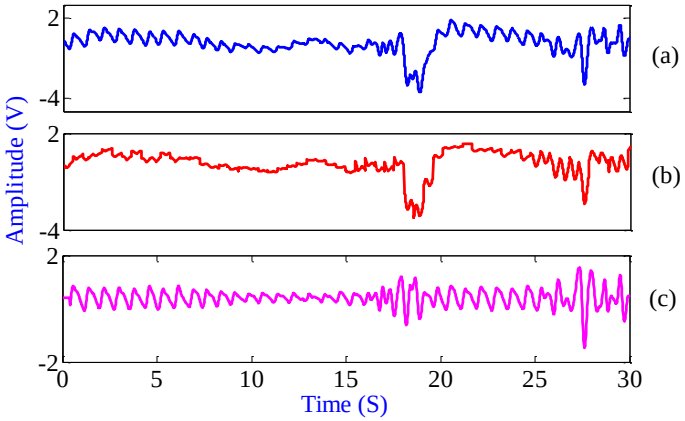

Fig. 5 – *PPG data:* (a) *signal corrupted with out-of-band noise;*
(b) *the generated inherent noise reference signal;*
(c) *data after noise elimination using the proposed technique.*

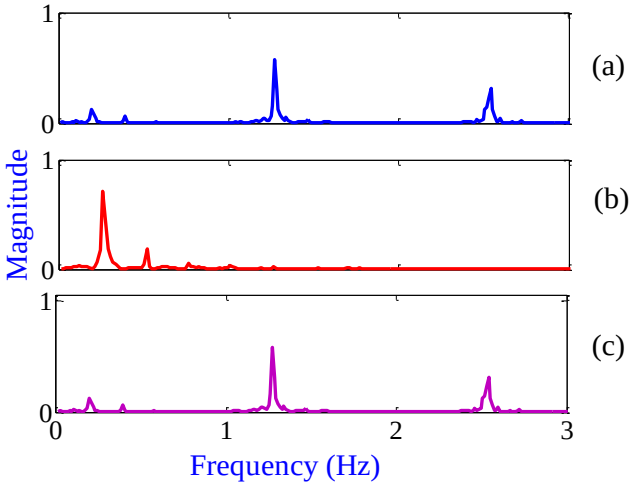

Fig. 6 – *Spectra for:* (a) *acquired PPG data with out-of-band noise;*
(b) *The generated inherent noise reference signal;*
(c) *PPG data after noise elimination using the proposed technique.*

The corresponding spectra are shown in Fig. 6. From Fig. 6b, it can be seen that the generated inherent noise reference appears as an out-of-band component, and this component is reduced to a greater extent in the de-noised spectrum Fig. 6c.

ii. If only in-band noise is present in the signal x2(n)

The kurtosis values for the approximate (A_j) and detail (D_j) coefficients for an eight-level decomposed signal $x_2(n)$ are presented in **Table 2**.

Table 2
Kurtosis values for the approximate and detail coefficients for the case of in-band noise only.

Coefficient	Kurtosis
D_1	8.55
D_2	6.39
D_3	8.41
D_4	3.92
D_5	4.67
D_6	4.33
D_7	5.53
D_8	4.22
A_8	4.73

The kurtosis values for all coefficients are between three and 10, representing both signal and noise, meaning that this situation resembles the case of in-band noise. Compared to the other coefficients, coefficient D_4 is closest to three, and therefore represents a possible pulsatile component. Thresholding is then applied to all coefficients to generate a noise reference signal for the adaptive filtering process.

Wavelet reconstruction is performed on the modified coefficients to generate an INR for the adaptive filtering process. The results discussed above are shown in Fig. 7. The PPG signal corrupted with most prominent in-band noise is presented in Fig. 7a, while the inherent out-of-band noise generated with a WT is shown in Fig. 7b and the corresponding de-noised PPG signal using the proposed adaptive filtering method is shown in Fig. 7c. Their corresponding spectra are shown in Fig. 8.

Fig. 8 shows a representative example of the efficacy of the proposed method. The generated in-band noise reference, shown in Fig. 8b, helps in reducing the MAs in the PPG signal, as shown in Fig. 8c, while at same time enhancing the signal quality, and clearly restores the respiratory signal. In practice, most existing MA reduction methods eliminate the respiratory component present in the PPG in the process of MA reduction.

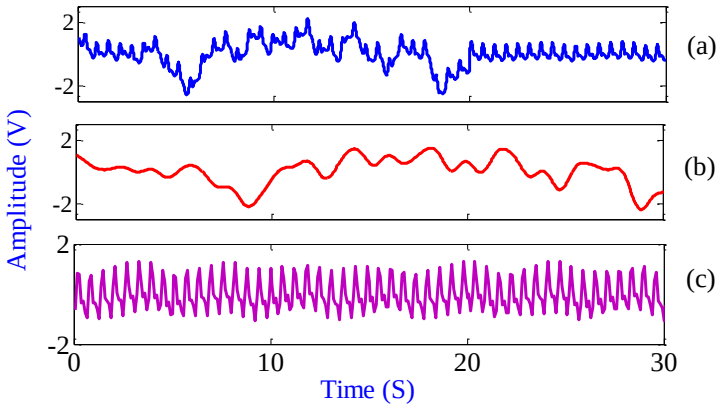

Fig. 7– (a) *PPG data corrupted with in-band noise;*
(b) *generated inherent noise reference signal;*
(c) *PPG data after noise elimination using the proposed technique.*

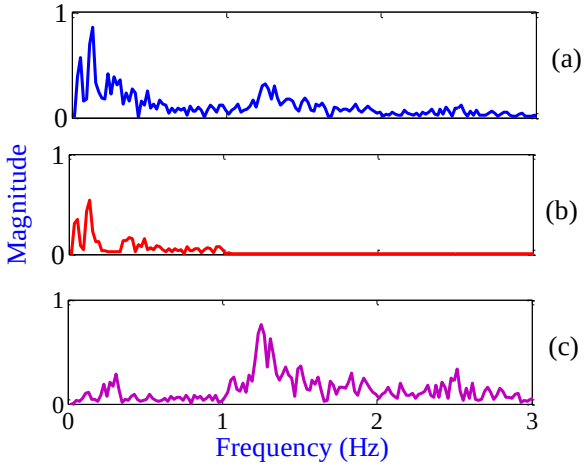

Fig. 8 – *Spectra for:* (a) *PPG signal corrupted with in-band noise;*
(b) *generated inherent noise reference signal;*
(c) *PPG data after noise elimination using the proposed technique.*

iii. If both in-band and out-of-band noise is present in the signal x3(n)

The kurtosis values for A_j and D_j for an eight-level decomposed PPG signal $x_3(n)$ consisting of both in-band and out-of-band noise are presented in **Table 3**. Here, the kurtosis values for the coefficients D_1, D_2 and D_3 are greater than 10, representing out-of-band noise. Of all the values, the kurtosis of D_4 is smallest, meaning that it represents the PPG pulsatile component. The kurtosis for remaining coefficients is greater than three and less than 10. Thresholding is

therefore applied to the coefficients A_8 and D_4 to D_8. Wavelet reconstruction is performed on the modified coefficients to generate a noise reference signal for the adaptive filtering process, representing both in-band and out-of-band noise.

Table 3

Kurtosis values for the approximate and detail coefficients for both in-band and out-of-band noise.

Coefficient	Kurtosis
D_1	31.67
D_2	27.81
D_3	18.37
D_4	4.34
D_5	4.67
D_6	4.76
D_7	5.53
D_8	4.22
A_8	4.73

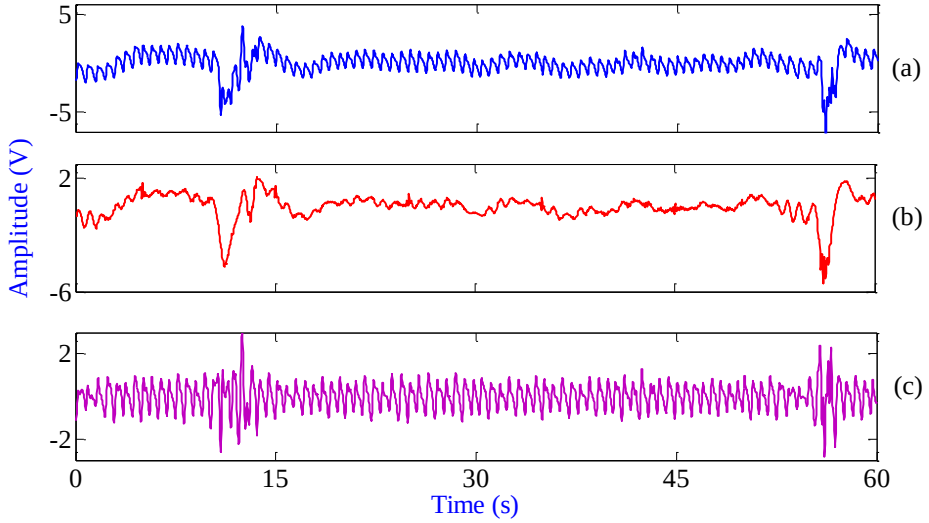

Fig. 9 – (a) *Acquired PPG data with in-band and out-of-band noise;* (b) *generated inherent noise reference signal;* (c) *PPG data after noise elimination using the proposed technique.*

The results discussed above are shown in Fig. 9. The PPG signal corrupted with a combination of both in-band and out-of-band noise is presented in Fig. 9a, while the inherent out-of-band noise generated with a WT is shown in Fig. 9b,

and the PPG signal after de-noising using the proposed adaptive filtering method is shown in Fig. 9c.

Their corresponding spectra are shown in Fig. 10, which provides another representative example of the efficacy of the proposed method. The generated INR, with both in-band and out-of-band noise, as shown in Fig. 10b, participating in the adaptive filtering, effectively reduces the MAs in the PPG signal, as shown in Fig. 10c, while preserving the respiratory component.

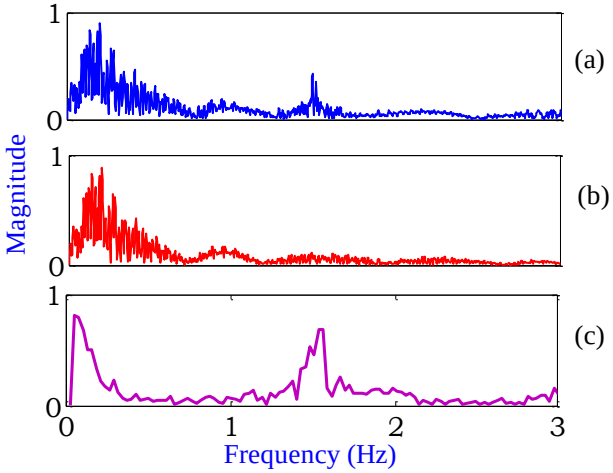

Fig. 10 – *Spectra for:* (a) *PPG signal corrupted with in-band and out-of-band noise;* (b) *generated inherent noise reference signal;* (c) *PPG data after noise elimination using the proposed technique.*

To further explore the efficacy of the proposed method for the case of a PPG signal corrupted with a combination of in-band and out-of-band noise, the corresponding wavelet-decomposed approximate and detail coefficients are shown in Fig. 11.

From **Table 3**, we see that the coeffficients D_1, D_2 and D_3 represent out-of-band MA noise. The same observation can clearly be made from the plots of D_1, D_2 and D_3 in Figs. 11 and 12. An important point here relates to D_4, as its kurtosis value reveals this to be a periodic signal representing the pulsatile component and some in-band noise component. It is interesting to note that this is evident from both the time domain plot of D_4 in Fig. 11 and the frequency domain plot in Fig. 12.

The kurtosis values for D_5 to D_8 and A_8 reveal that they correspond to random components but with other hidden periodic components of the signal. Hence, thresholding will be applied to D_4 to D_8 and A_8, to generate the in-band reference noise. This well-defined process generates a reliable INR for effective adaptive filtering.

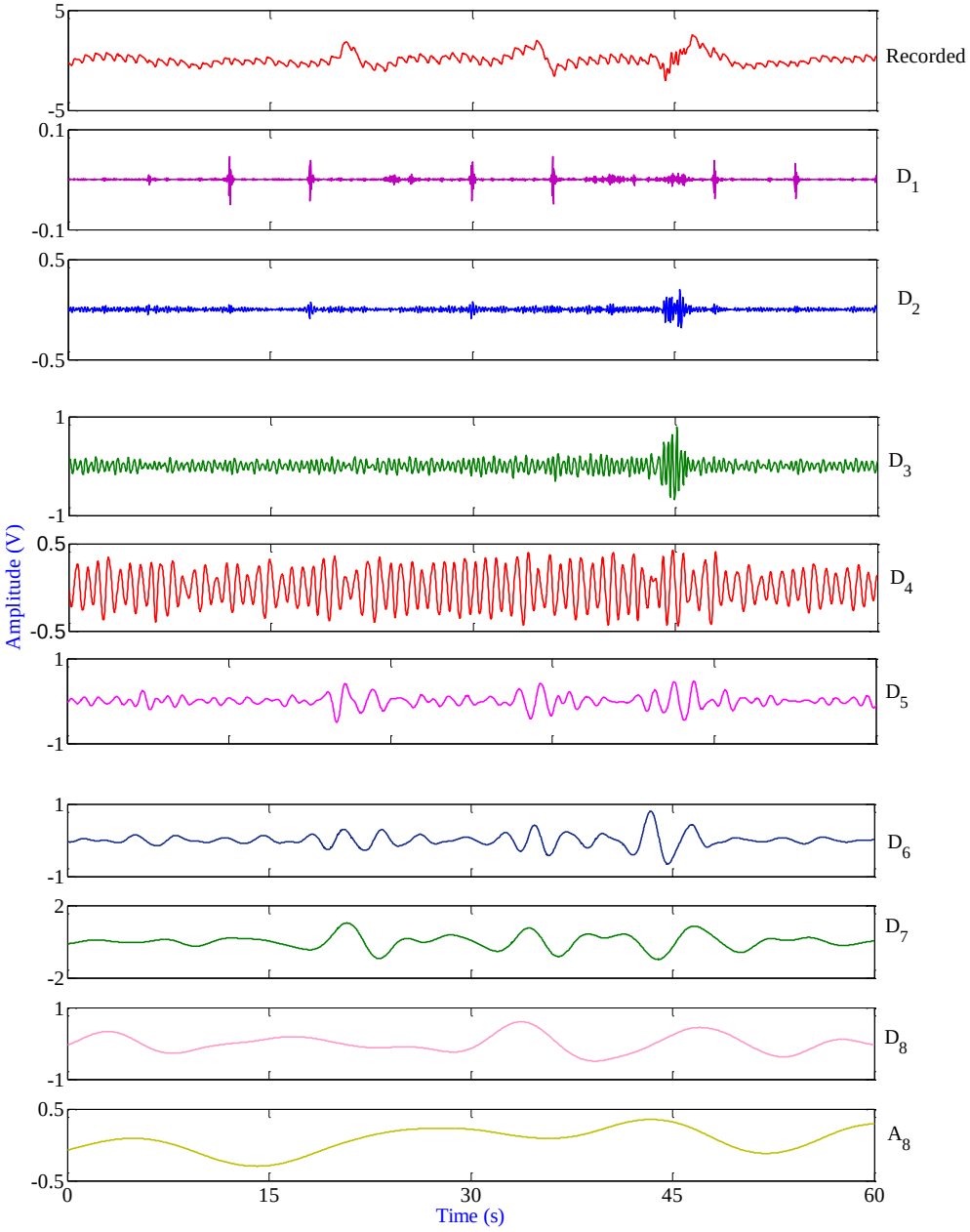

Fig. 11 – *Time domain plot of a noisy PPG signal and signals reconstructed from the wavelet coefficients: approximate (Aj) and detail (Dj).*

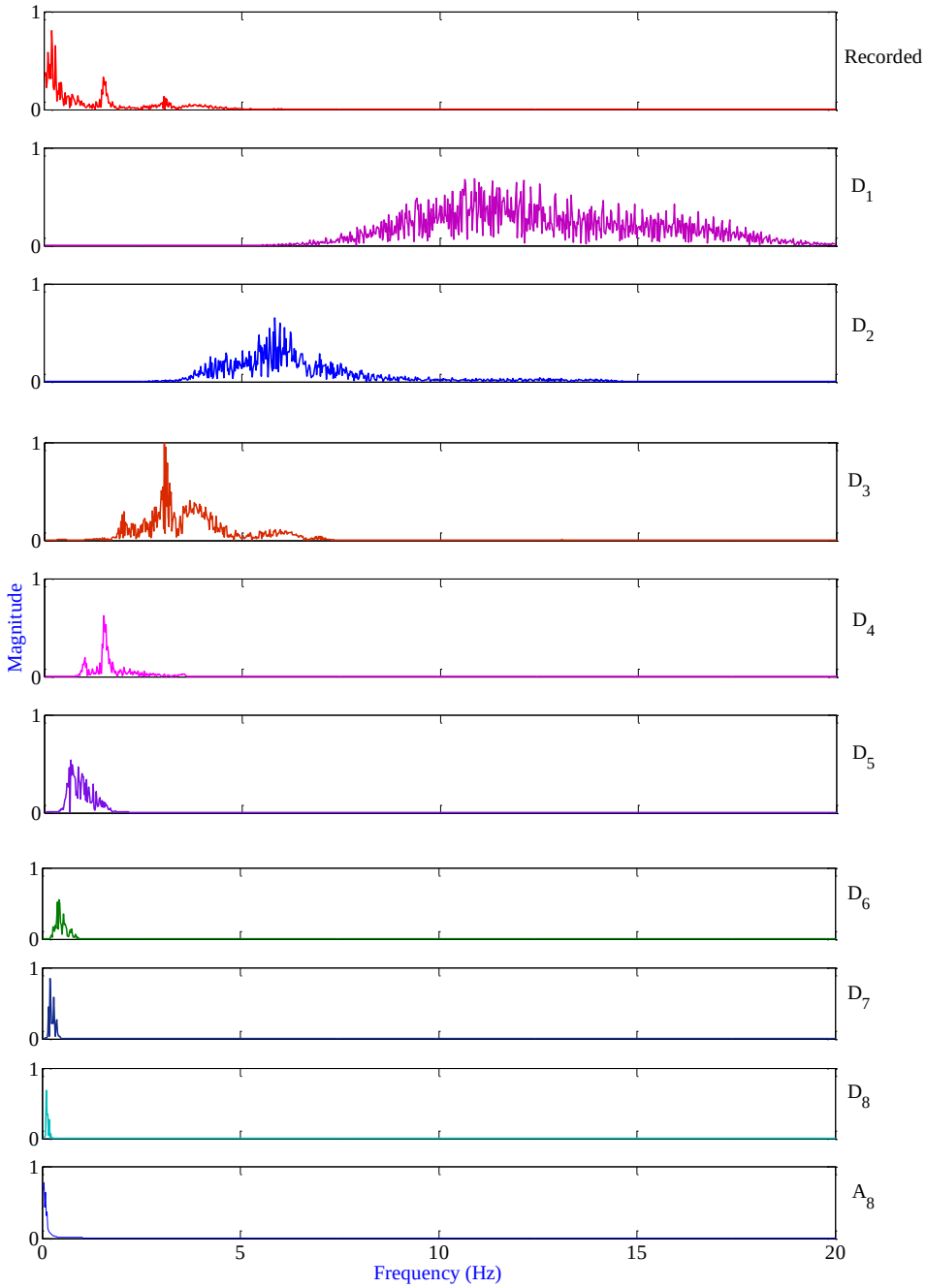

Fig. 12 – *Frequency domain plots of noisy PPG signals and spectra for the reconstructed signals from the wavelet coefficients: approximate (Aj) and detail (Dj).*

After establishing the validity of the generated INR, the complete method was applied to corrupted PPG signals. The results are depicted in Figs. 13 and 14.

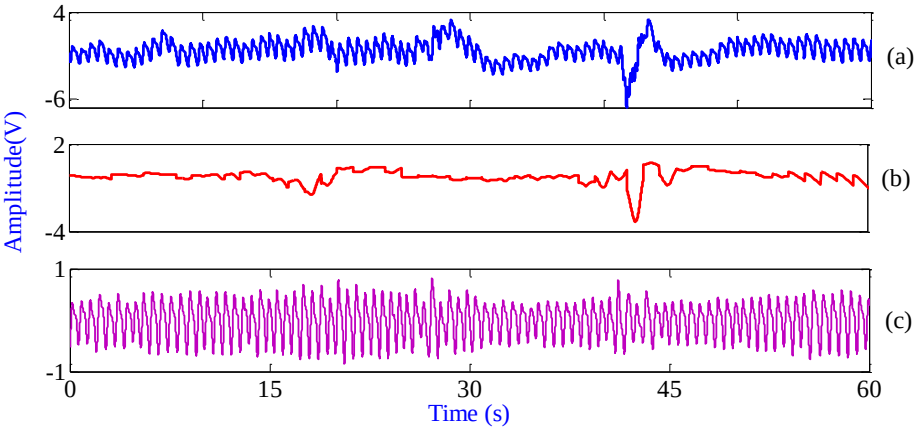

Fig. 13 – (a) *Noisy pulse oximeter data with* ***vertical MAs of the finger****;*
(b) *inherent noise reference signal reconstructed using wavelet transform;*
(c) *pulse oximeter data after noise elimination using the proposed methodology.*

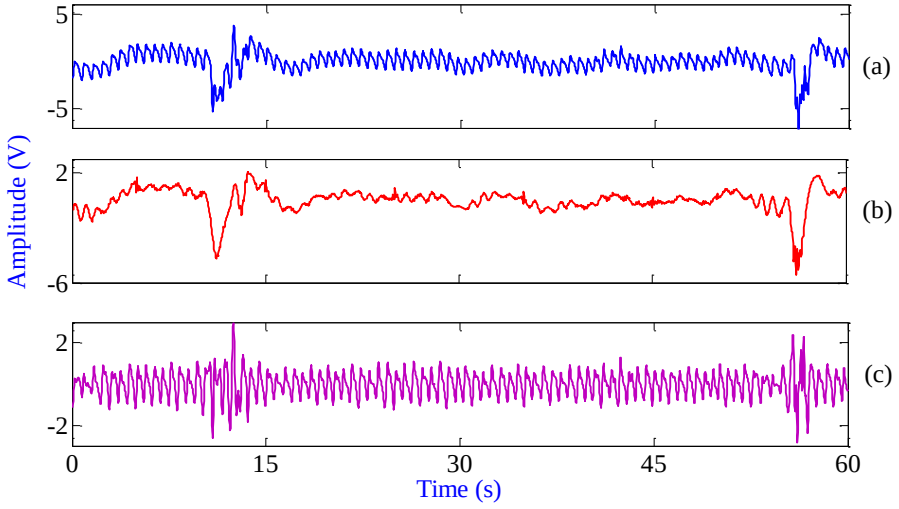

Fig. 14 – (a) *Noisy pulse oximeter data with horizontal MAs of the finger;*
(b) *inherent noise reference signal reconstructed using wavelet transform;*
(c) *pulse oximeter data after noise elimination using the proposed methodology.*

A pulse oximeter PPG signal with vertical MAs is shown in Fig. 13a. The acquired PPG data were modified using the proposed methodology, and the INR signal generated in this way, shown in Fig. 13b, was used for further processing

with the adaptive filter. It was established that the adaptive step size LMS (AS-LMS) algorithm yielded improved convergence compared to the other variants of LMS adaptive filtering. The pulse oximeter signal after noise elimination is shown in Fig. 13c. Similar results are found from an analysis of pulse oximeter PPG data with horizontal MAs, as presented in Fig. 14.

4 Discussion

Statistical Analysis

The DC and AC component values of the red and IR PPG cycles are required in order to estimate the SpO_2. The peak-to-peak values of the pulsatile components of the red and IR PPG signals are used to first compute the "ratio of ratios" R and then to estimate the SpO_2 values [15], as shown below:

$$R = \frac{(AC_{\mathrm{Red}}/DC_{\mathrm{Red}})}{(AC_{IR}/DC_{IR})}, \tag{7}$$

$$SpO_2\% = (110 - 25R)\%. \tag{8}$$

As the MAs disturb the peak-to-peak values of the PPG cycles, the extent to which the cycles are disturbed is observed by computing the mean ± standard deviation (SD) for the peak-to-peak values of the recovered PPG cycles. The results in **Table 4** reveal that the peak-to-peak values for the PPG signal recovered using the proposed method are very close to the clean portion of the PPG signal, thus illustrating the robustness of our approach. These restored peak-to-peak values can then be used to estimate SpO2, as shown in (8).

Table 4
Peak-to-peak values of pulse oximeter data.

PPG	Horizontal motion	Vertical motion	Bending motion
Clean section	**0.370±0.024**	**0.427±0.044**	**0.356±0.021**
Corrupted section	0.425±0.086	0.513±0.106	0.458±0.066
Section recovered using WTB-AF	**0.394±0.048**	**0.471±0.056**	**0.389±0.046**

It is a very good indicator to assess the potential of the method, since estimation of SpO_2 depends on that. The values of SpO_2 in **Table 5** that were estimated using the proposed method are nearly equal to the values for the clean PPG section, thus illustrating the efficacy of the proposed method, which has a worst-case accuracy of 0.5%.

Table 5
Computed SpO2 values.

PPG	SpO_2 % estimation		
	Horizontal motion	**Vertical motion**	**Bending motion**
Clear portion	**97.8**	**96.9**	**98.1**
Corrupted section	94.1	95.2	95.7
Section recovered using WTB-AF	**97.4**	**96.4**	**97.6**
Accuracy	**0.4%**	**0.5%**	**0.5%**

Finally, to assess the validity of the generated reference signal using statistical measures, time-domain and frequency-domain similarity measures were computed as follows. The correlation coefficient (CC) is defined as

$$C_{XY} = \frac{\text{cov}(X,Y)}{\sigma_X \, \sigma_Y} = \frac{\sum_{i=1}^{n}(x_i - \bar{x})(y_i - \bar{y})}{\sqrt{\sum_{i=1}^{n}(x_i - \bar{x})^2}\sqrt{\sum_{i=1}^{n}(y_i - \bar{y})^2}}, \tag{9}$$

where $\text{cov}(X,Y)$ represents the covariance between X and Y; and σ_X, σ_Y represent the standard deviation in X and Y, respectively.

The values of *CC* were computed between the noisy PPG, noise reference and de-noised PPG signals, and the results are presented in **Table 7**.

CC_{NPRS} represents the CC between the noisy PPG signal (NP) and noise reference signal (RS). This coefficient should show 50% similarity.

CC_{NPDP} represents the CC between the noisy PPG signal (NP) and the de-noised PPG signal (DP). This coefficient should show a similarity of around 70%.

CC_{RSDP} represents the CC between the noise reference signal (RS) and the de-noised PPG signal (DP). This coefficient should show minimal similarity.

The frequency-domain measure is defined as

$$MSC = \frac{\left|S_{xy}(k)\right|^2}{S_{xx}(k)\,S_{yy}(k)}, \tag{10}$$

where $S_{xy}(k)$ is the cross-power spectral density of x and y, and $S_{xx}(k)$ and $S_{yy}(k)$ are the auto-power spectral densities of x and y, respectively.

A frequency-domain measure called the magnitude squared coherence (MSC) is computed as follows:

– MSC_{NPRS} represents the MSC between the noisy PPG (NP) signal and the noise reference signal (RS). This coefficient should show a 50% similarity.
– MSC_{NPDP} represents the CC between the noisy PPG (NP) and the de-noised PPG signal (DP). This coefficient should show a similarity of around 70%.
– MSC_{RSDP} represents the CC between the noise reference signal (RS) and the de-noised PPG signal (DP). This coefficient shall show minimal similarity.

From the computed CC values for different MAs in **Table 6**, it can be observed that the value of CC_{NPRS}, which is greater than 0.5 and less than 0.6, indicates a similarity of greater than 50% between the noisy PPG signal and the noise reference signal. Similarly, the value of CC_{NPDP} indicates that a similarity of nearly 70% can be seen between the noisy and PPG signals. Finally, as expected, the CC_{RSDP} reveals little correlation between noise reference signal and the de-noised PPG signal. The results for the frequency-domain MSC presented in **Table 7** also confirm the validity of the generated inherent noise reference.

Table 6
Calculated values of CC for different motion artifacts.

	Vertical motion	**Horizontal motion**	**Bending motion**
CC_{NPRS}	0.54	0.58	0.59
CC_{NPDP}	0.72	0.73	0.68
CC_{RSDP}	0.08	0.06	0.07

Table 7
Calculated values of MSC for different motion artifacts.

	Vertical motion	**Horizontal motion**	**Bending motion**
MSC_{NPRS}	0.52	0.54	0.56
MSC_{NPDP}	0.83	0.79	0.76
MSC_{RSDP}	0.09	0.08	0.11

The results and the discussion presented above prove the validity of the INR signal and the efficacy of the proposed method of reducing MAs from PPG signals to achieve reliable SpO2 estimations.

5 Conclusion

In this work, we have presented an effective adaptive filtering method using a WT for the elimination of MAs from pulse oximeter signals. Most existing adaptive MA reduction methods use an additional sensor to capture the MAs for

use as a reference signal for adaptive filtering. Our proposed method dispenses with the additional sensor, and inherently generates a noise reference from the corrupted PPG data using an efficient wavelet-based decomposition method. The INR generated in this way can be used with an adaptive step size LMS (AS-LMS) method of adaptive filtering, for the efficient reduction of MAs. Our approach was validated using time domain and frequency domain measures, and was found to give reliable SpO_2 estimations with a worst-case accuracy of 0.5%. The most notable aspect of our method is that it restored the respiratory signal present in the PPG while efficiently reducing the MAs.

6 References

[1] J. Allen: Photoplethysmography and Its Application in Clinical Physiological Measurement, Physiological Measurement, Vol. 28, No. 3, February 2007, pp. R1 – R39.

[2] M. T. Petterson, V. L. Begnoche, J. M. Graybeal: The Effect of Motion on Pulse Oximetry and Its Clinical Significance, Anesthesia & Analgesia, Vol. 105, No. 6, December 2007, pp. S78 – S84.

[3] T. Tamura, Y. Maeda, M. Sekine, M. Yoshida: Wearable Photoplethysmographic Sensors – Past and Present, Electronics, Vol. 3, No. 2, April 2014, pp. 282 – 302.

[4] T. Tamura: Current Progress of Photoplethysmography and SPO_2 for Health Monitoring, Biomedical Engineering Letters, Vol. 9, February 2019, pp. 21 – 36.

[5] Q. Xiaoyan, Y. Feng, D. Youer: Motion Artifact Elimination Using Adaptive Filter Based on Wavelet Transform in Pulse Wave Measurement, Proceedings of the IEEE International Conference on Intelligent Computing and Intelligent Systems, Shanghai, China, November 2009, pp. 319 – 322.

[6] B. Lee, Y. Kee, J. Han, W. J. Yi: Adaptive Comb Filtering for Motion Artifact Reduction from PPG with a Structure of Adaptive Lattice IIR Notch Filter, Proceedings of the Annual International Conference of the IEEE Engineering in Medicine and Biology Society, Boston, USA, August 2011, pp. 7937 – 7940.

[7] R. Yousefi, M. Nourani, I. Panahi: Adaptive Cancellation of Motion Artifact in Wearable Biosensors, Proceedings of the Annual International Conference of the IEEE Engineering in Medicine and Biology Society, San Diego, USA, August 2012, pp. 2004 – 2008.

[8] F. Peng, Z. Zhang, X. Gou, H. Liu, W. Wang: Motion Artifact Removal from Photoplethysmographic Signals by Combining Temporally Constrained Independent Component Analysis and Adaptive Filter, BioMedical Engineering OnLine 2, Vol. 13, April 2014, p. 50.

[9] K. A. Reddy, B. George, V. J. Kumar: Use of Fourier Series Analysis for Motion Artifact Reduction and Data Compression of Photoplethysmographic Signals, IEEE Transactions on Instrumentation and Measurement, Vol. 58, No. 5, May 2009, pp. 1706 – 1711.

[10] Q. Wang, P. Yang, Y. Zhang: Artifact Reduction Based on Empirical Mode Decomposition (EMD) in Photoplethysmography for Pulse Rate Detection, Proceedings of the Annual International Conference of the IEEE Engineering in Medicine and Biology, Buenos Aires, Argentina, August 2010, pp. 959 – 962.

[11] M. Raghuram, K. Sivani, K. A. Reddy: MS-EMD Based Signal Processing Method for Reduction of Motion Artifacts from PPG Signals, International Journal of Applied Engineering Research, Vol. 13, No. 21, 2018, pp. 14969 – 14973.

[12] H.- W. Lee, J.- W. Lee, W.- G. Jung, G.- K. Lee: The Periodic Moving Average Filter for Removing Motion Artifacts from PPG Signals, International Journal of Control, Automation and Systems, Vol. 5, No. 6, December 2007, pp. 701 – 706.

[13] T. Bai, D. Li, H. Wang, Y. Pang, G. Li, J. Lin, Q. Zhou, G. Jeon: A PPG Signal De-Noising Method Based on the DTCWT and the Morphological Filtering, Proceedings of the 12th International Conference on Signal-Image Technology & Internet-Based Systems (SITIS), Naples, Italy, November 2016, pp. 503 – 506.

[14] F. Peng, H. Liu, W. Wang: A Comb Filter Based Signal Processing Method to Effectively Reduce Motion Artifacts from Photoplethysmographic Signals, Physiological Measurement, Vol. 36, No. 10, October 2015, pp. 2159 – 2170.

[15] S. M. A. Salehizadeh, D. Dao, J. Bolkhovsky, C. Cho, Y. Mendelson, K. H. Chon: A Novel Time-Varying Spectral Filtering Algorithm for Reconstruction of Motion Artifact Corrupted Heart Rate Signals During Intense Physical Activities Using a Wearable Photoplethysmogram Sensor, Sensors, Vol. 16, No. 1, December 2015, p. 10.

[16] K. T. Tanweer, S. R. Hasan, A. M. Kamboh: Motion Artifact Reduction from PPG Signals During Intense Exercise Using Filtered X-LMS, Proceedings of the IEEE International Symposium on Circuits and Systems (ISCAS), Baltimore USA, May 2017, pp. 1 – 4.

[17] M. S. Roy, R. Gupta, J. K. Chandra, K. D. Sharma, A. Talukdar: Improving Photoplethysmographic Measurements Under Motion Artifacts Using Artificial Neural Network for Personal Healthcare, IEEE Transactions on Instrumentation and Measurement, Vol. 67, No. 12, December 2018, pp. 2820 – 2829.

[18] Q. Zhang, Q. Xie, M. Wang, G. Wang: Motion Artifact Removal for PPG Signals Based on Accurate Fundamental Frequency Estimation and Notch Filtering, Proceedings of the 40th Annual International Conference of the IEEE Engineering in Medicine and Biology Society (EMBC), Honolulu, USA, July 2018, pp. 2965 – 2968.

[19] A. Luke, S. Shaji, K. A. U. Menon: Motion Artifact Removal and Feature Extraction from PPG Signals Using Efficient Signal Processing Algorithms, Proceedings of the International Conference on Advances in Computing, Communications and Informatics (ICACCI), Bangalore, India, September 2018, pp. 624 – 630.

[20] M. Raghu Ram, K. Venu Madhav, E. Hari Krishna, N. Raddy Komalla, K. Ashoka Reddy: A Novel Approach for Motion Artifact Reduction in PPG Signals Based on AS-LMS Adaptive Filter, IEEE Transactions on Instrumentation and Measurement, Vol. 61, No. 5, May 2012, pp. 1445 – 1457.

[21] J. Xiong, L. Cai, D. Jiang, H. Song, X. He: Spectral Matrix Decomposition-Based Motion Artifacts Removal in Multi-Channel PPG Sensor Signals, IEEE Access, Vol. 4, 2016, pp. 3076 – 3086.

[22] E. Khan, F. Al Hossain, S. Z. Uddin, S. K. Alam, M. K. Hasan: A Robust Heart Rate Monitoring Scheme Using Photoplethysmographic Signals Corrupted by Intense Motion Artifacts, IEEE Transactions on Biomedical Engineering, Vol. 63, No. 3, March 2016, pp. 550 – 562.

[23] R. W. C. G. R. Wijshoff, M. Mischi, R. M. Aarts: Reduction of Periodic Motion Artifacts in Photoplethysmography, IEEE Transactions on Biomedical Engineering, Vol. 64, No. 1, January 2017, pp. 196 – 207.

[24] W. Kang, M. Li, X. Che, J. Wang, F. Lai: Pulse Rate Estimation Using PPG Affected with Motion Artifacts Based on VMD and Hilbert Transform, Proceedings of the IEEE International Conference on Robotics and Biomimetics (ROBIO), Dali, China, December 2019, pp. 2676 – 2681.

[25] J. Harvey, S. M. A. Salehizadeh, Y. Mendelson, K. H. Chon: OxiMA: A Frequency-Domain Approach to Address Motion Artifacts in Photoplethysmograms for Improved Estimation of Arterial Oxygen Saturation and Pulse Rate, IEEE Transactions on Biomedical Engineering, Vol. 66, No. 2, February 2019, pp. 311 – 318.

[26] K. Xu, X. Jiang, W. Chen: Photoplethysmography Motion Artifacts Removal Based on Signal-Noise Interaction Modeling Utilizing Envelope Filtering and Time-Delay Neural Network, IEEE Sensors Journal, Vol. 20, No. 7, April 2020, pp. 3732 – 3744.

[27] S. Nabavi, S. Bhadra: A Robust Fusion Method for Motion Artifacts Reduction in Photoplethysmography Signal, IEEE Transactions on Instrumentation and Measurement, Vol. 69, No. 12, December 2020, pp. 9599 – 9608.

[28] S. Alam, R. Gupta, K. Das Sharma: On-Board Signal Quality Assessment Guided Compression of Photoplethysmogram for Personal Health Monitoring, IEEE Transactions on Instrumentation and Measurement, Vol. 70, 2021, p. 4003809.

[29] N. De Pinho Ferreira, C. Gehin, B. Massot: Ambient Light Contribution as a Reference for Motion Artefacts Reduction in Photoplethysmography, Proceedings of the 13th International Conference on Biomedical Electronics and Devices, Valletta, Malta, February 2020, pp. 23 – 32.

[30] B. Venumaheswar Rao, K. Ashoka Reddy: On the Use of Wavelet Transform Based Adaptive Filtering for De-Noising of Pulse Oximeter Signals, Proceedings of the IEEE International Instrumentation and Measurement Technology Conference (I2MTC), Glasgow, UK, May 2021, pp. 1 – 4.

[31] H. H. Asada, H.- H. Jiang, P. Gibbs: Active Noise Cancellation Using MEMS Accelerometers for Motion-Tolerant Wearable Bio-Sensors, Proceedings of the 26th Annual International Conference of the IEEE Engineering in Medicine and Biology Society, San Francisco, USA, September 2004, pp. 2157 – 2160.

[32] P. Gibbs, H. H. Asada: Reducing Motion Artifact in Wearable Bio-Sensors Using MEMS Accelerometers for Active Noise Cancellation, Proceedings of the American Control Conference (ACC), Portland, USA, June 2005, pp. 1581 – 1586.

[33] J. Shin, J. Cho: Noise-Robust Heart Rate Estimation Algorithm from Photoplethysmography Signal with Low Computational Complexity, Journal of Healthcare Engineering, Vol. 2019, May 2019, p. 6283279.

[34] A. H. A. Zargari, S. A. H. Aqajari, H. Khodabandeh, A. M. Rahmani, F. Kurdahi: An Accurate Non-Accelerometer-Based PPG Motion Artifact Removal Technique Using CycleGAN, arXiv:2106.11512 [cs.LG], June 2021, pp. 1 – 12.

[35] B. Widrow, M. E. Hoff: Adaptive Switching Circuits, Proceedings of the IRE WESCON Convention Record, New York, USA, June 1960, pp. 96 – 104.

[36] I. Daubechies: The Wavelet Transform, Time-Frequency Localization and Signal Analysis, IEEE Transactions on Information Theory, Vol. 36, No. 5, September 1990, pp. 961 – 1005.